The Astrophysical Journal, 860:26 (7pp), 2018 June 10 https://doi.org/10.3847/1538-4357/aabba3

Torsional Alfvén Wave Embedded ICME Magnetic Cloud and Corresponding Geomagnetic Storm

Anil N. Raghav[1], Ankita Kule[1], Ankush Bhaskar[2,3], Wageesh Mishra[4], Geeta Vichare[5], and Shobha Surve[6]
[1] University Department of Physics, University of Mumbai, Vidyanagari, Santacruz (E), Mumbai-400098, India; raghavanil1984@gmail.com
[2] Heliophysics Science Division, NASA/Goddard Space Flight Center, Greenbelt, MD, USA
[3] University Corporation for Atmospheric Research, Boulder, CO, USA
[4] University of Science and Technology of China, Hefei, Anhui, People's Republic of China
[5] Indian Institute of Geomagnetism, Navi Mumbai, India
[6] Centre for Excellence in Basic Sciences, Mumbai, India
Received 2018 March 1; revised 2018 March 27; accepted 2018 March 29; published 2018 June 7

Abstract

Energy transfer during the interaction of large-scale solar wind structure and the Earth's magnetosphere is a chronic issue in space-weather studies. To understand this, researchers widely studied the geomagnetic storm and substorm phenomena. The present understanding suggests that the long duration of the southward interplanetary magnetic field component is the most important parameter for the geomagnetic storm. Such a long duration strong southward magnetic field is often associated with ICMEs, torsional Alfvén fluctuations superposed corotating interacting regions (CIRs), and fast solar wind streams. Torsional Alfvén fluctuations embedded CIRs have been known of for a long time; however, magnetic clouds embedded with such fluctuations are rarely observed. The presence of Alfvén waves in the ICME/MC and the influence of these waves on the storm evolution remains an interesting topic of study. The present work confirms the torsional Alfvén waves in a magnetic cloud associated with a CME launched on 2011 February 15, which impacted the Earth's magnetosphere on 2011 February 18. Furthermore, observations indicate that these waves inject energy into the magnetosphere during the storm and contribute to the long recovery time of geomagnetic storms. Our study suggests that the presence of torsional Alfvén waves significantly controls the storm dynamics.

Key words: magnetohydrodynamics (MHD) – solar–terrestrial relations – solar wind – Sun: coronal mass ejections (CMEs) – Sun: heliosphere

1. Introduction

In the present satellite era, the study of space physics has become of paramount importance as space-weather events can disturb our day-to-day activities. Geomagnetic storms, i.e., the temporary disturbances in the Earth's magnetosphere (Gonzalez et al. 1994; Tsurutani et al. 1995a; Lakhina et al. 2007), are one of such events that can lead to a serious of adverse effects on communication, navigation, and electrical systems (Carrington 1859; Osella et al. 1998; Tsurutani et al. 2003; Schrijver & Siscoe 2010; Cannon et al. 2013; Gawali et al. 2016; Lakhina & Tsurutani 2016). In general, the southward oriented interplanetary magnetic field (IMF) in combination with a strong, high speed solar wind stream are considered to be a main driver of a geomagnetic storm (Tsurutani et al. 1992, 1995a; Gonzalez et al. 1999; Vichare et al. 2005). Whereas a viscous type of interactions of high speed solar wind with a magnetosphere are also considered when the IMF is northward (Axford 1964). However, the energy transferred to the magnetosphere through this is very small and therefore, it is no longer believed to be geoeffective for creating geomagnetic storms (Tsurutani & Gonzalez 1995; Du et al. 2008). The negative B_z component interacts with Earth's magnetic field via magnetic reconnection and the charged particles penetrate into the Earth's magnetosphere from the day-side of the magnetosphere (Gonzalez et al. 1994). Most of the particles are injected into the inner magnetosphere because of plasma sheet reconnection at the magnetotail (Behannon & Ness 1966). Due to the gradient and curvature of the Earth's magnetic field, injected particles, e.g., protons drift toward the west and electrons toward the east, such that the westward ring current is set up. The magnetic moment of the ring current is in the opposite direction as that of the Earth's magnetic dipole moment. Thus, a negative magnetic field perturbation, i.e., a depression is observed at the ground.

The literature on the geomagnetic effects of solar wind structures identify three major causes of geomagnetic storms: (i) coronal mass ejections (CMEs); (2) corotating interaction regions (CIRs); and (3) the Alfvén waves superposed high speed solar wind streams (Parker 1958; Tsurutani et al. 1988; Cane & Richardson 1997; Tsurutani & Gonzalez 1997; Borovsky & Denton 2006; Tsurutani et al. 2006). The CME-driven storms are frequently stronger with significantly enhanced ring currents that induce great auroras. The CIR-driven storms are normally moderate/weaker with less intensive auroras (Tsurutani & Gonzalez 1997; Borovsky & Denton 2006). The geomagnetic storm comprises various phases viz. sudden storm commencement (SSC) or gradual commencement (GC), initial phase, main phase, and recovery phase of the storm (Tsurutani & Gonzalez 1997; Gonzalez et al. 1999). The SSC and/or GC are mainly controlled by the solar wind dynamic pressure, i.e., initiated by the forward shock-front of CME. In CME-driven storms, the main phase is caused by a southward IMF, which directly contributes to the increase in ring current, whereas the recovery starts when ring currents begin to decay. Thus CME-driven storms only last for a few days (Borovsky & Denton 2006).

Compared to this, the CIR and high speed stream (HSS) from coronal-hole-driven magnetic storms can last from a few days up to a few weeks (Tsurutani et al. 2006), generally known as High Intensity Long Duration Continuous AE

Activity (HILDCAAs) events (Tsurutani & Gonzalez 1987; Hajra et al. 2013, 2014, 2015; Prestes et al. 2017). The CIR occurs at the interface between the HSS and the upstream slow stream (Smith & Wolfe 1976; Burlaga & Lepping 1977; Gonzalez et al. 1999). The amplified Alfvénic fluctuations are observed within CIRs as well as the HSSs that trail the CIR (has lower amplitude Alfvén waves). Magnetic reconnection between the southward component of the Alfvén waves and the magnetosphere fields slowly inject solar wind energy and plasma into the magnetosphere, which causes the extended recoveries of the storms (Tsurutani et al. 1995b; Tsurutani et al. 2006).

Although Alfvén waves are very common in space plasmas, it is rare to obtain their spatial picture. This is because Alfvén waves are slowly varying and have very long wavelengths along the magnetic field. Due to the torsional wave, there are no fluctuations in the fluid density, and hence no variations in the observed emission intensity images and thus they are more difficult to observe. However, based on the spectrometric studies of solar corona, the presence of Alfvén waves is inferred (Banerjee et al. 1998; Harrison et al. 2002; Banerjee et al. 2009). Recently, Tian et al. (2010) proposed that Alfvénic fluctuations are observed in flux ropes. Gosling et al. (2010) also suggested that a torsional wave could be generated by distortions within a flux rope ejected from the Sun. It is considered that (i) twisting in straight or homogeneous magnetic field lines, (ii) ejecting axial current at the base of pre-existing flux rope, or (iii) otherwise changing the force balance condition associated with pre-existing flux rope can generate Alfvén waves (Fan 2009; Gosling et al. 2010). Therefore, Alfvén waves are expected to be observed within magnetic cloud-like structures. However, they are not commonly observed within the magnetic clouds of various sizes in the solar wind. In earlier studies, Alfvénic wave fluctuations are observed in the region where fast and slow solar wind streams interact, i.e., CIRs region (Tsurutani et al. 1995b; Lepping et al. 1997). Furthermore, the presence of the Alfvén waves during interface of magnetic cloud and solar wind stream is observed (Behannon et al. 1991; Lepping et al. 1997). Recently, the presence of Alfvén waves embedded in the magnetic cloud is interpreted as the output of a CME–CME interaction (Raghav & Kule 2018). In the present work, we aim to study the presence of torsional Alfvén waves in the magnetic cloud (MC) and trailing region of the MC. It is not so common to observe Alfvén waves in the magnetic cloud. This motivates us to understand the geomagnetic storm characteristics associated with both aforementioned regions. Finally, we discuss the possible contribution of Alfvén waves in the storm and compare with past studies.

2. Observations

The event under study caused by the multiple-CMEs that erupted on 2011 February 13th, 14th, and 15th, interacted en route and appeared as a complex magnetic structure at 1 au in *WIND* satellite data. The selected event has been studied in the past to understand (1) their interaction corresponding to different position angles (Temmer et al. 2014), (2) their geometrical properties and the coefficient of restitution for the head-on collision scenario and their geomagnetic response (Mishra & Srivastava 2014), (3) corresponding Forbush decrease phenomena (Maričić et al. 2014; Raghav et al. 2014, 2017), and (4) the presence of Alfvén waves in the interacting region (Raghav & Kule 2018).

Figure 1 shows the in situ observation (in GSE-coordinate system) of the ICMEs with D_{st} index. The red lines depict the arrival time of the shock and the gray shades show the region of the ICME magnetic cloud. The top panel displays the magnitude of the magnetic field B (nT), which shows magnetic field enhancement and a gradual decrease in the shaded region. The second top panel consists of magnetic vectors B_x, B_y, and B_z, in which B_z shows no rotation, B_y shows slight rotation whereas B_x shows smooth variations in the shaded region. The third panel from the top consists of a θ angle that is relatively constant and the fourth panel consist of a ϕ angle that varies slowly in the shaded region. Hence, this suggests a magnetic cloud or magnetic cloud-like structure with relatively little rotation. It is also identified as a magnetic cloud in the Lepping MC list available at https://wind.gsfc.nasa.gov/mfi/mag_cloud_S1.html. The fifth panel shows pitch angle distribution of electrons that indicate the signature of the MC. The sixth panel displays gradually decreasing solar wind speed. The seventh panel demonstrates almost constant low proton density (Np). The eighth panel consists of the proton temperature on the left side and the ratio of the proton temperature observed to the expected proton temperature on the right, which is nearly 0.5 throughout the MC crossing. The second panel from the bottom displays less than 0.1 value of plasma beta within the MC boundaries. The bottom panel consists of the D_{st} index, which suggests overall the geomagnetic response to the observed MC. The long recovery phase with a moderate/weak type of storm is observed during the observed MC.

In Figure 2, regions 1 and 2 are specifically shown in shades of pink and green. The observed complex interplanetary structures before region 1 are explained at length in the literature (Maričić et al. 2014; Mishra & Srivastava 2014; Raghav & Kule 2018). Region 1 is shaded in pink and it is identified as an MC/MC-like structure. Similarly, Region 2 is (shaded in green) MC trailing solar wind. The third, forth, and fifth panels from the top demonstrate the temporal variation of the magnetic field and solar wind components in the GSE-coordinate system. The peculiar and distinct features of variation in all three components of B and V are seen in regions 1 and 2, i.e., the well-correlated changes in respective components of magnetic field B and solar wind speed V is observed. Raghav & Kule (2018) manifest this as the presence of Alfvén waves in MC, i.e., region 1. Furthermore, region 2 also shows a similar trend of variations that might be Alfvénic type. The bottom panel displays the temporal variations of longitudinal symmetric disturbance index SYM-H. It remains almost constant during complete passage of MC and suggests a weak/moderate disturbed condition with approximately -25 nT value. After MC crosses over, the SYM-H recovers to ~ 0 nT at 00: 00 UT on February 21 and further remains fluctuating in negative values in region 2.

To confirm the presence of Alfvén waves in region 1 and the possibility in region 2, the Walén relation is used. The Walén relation is described as

$$V_A = \pm A \frac{B}{\sqrt{\mu_0 \rho}}, \quad (1)$$

where A is the anisotropy parameter, B is the magnetic field vector, and ρ is proton mass density (Walén 1944; Hudson 1971). By considering negligible influence of the thermal

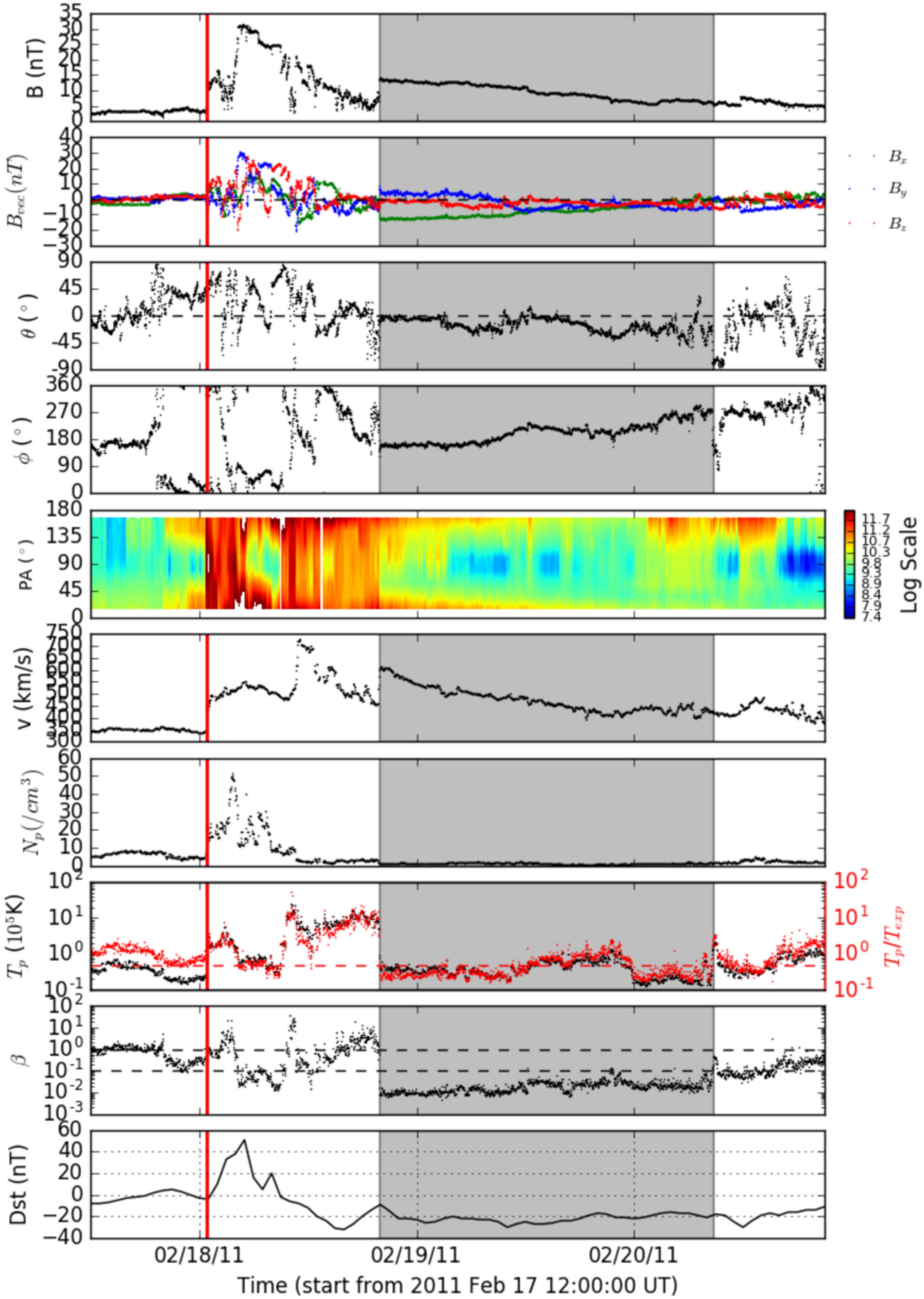

Figure 1. Interplanetary magnetic field (IMF), solar wind plasmas, and the suprathermal electron pitch angle distribution observations of the complex CME–CME interaction event crossed on 2011 February 18–19 from *WIND* spacecraft. From top to the bottom, parameters are the magnetic field strength (|*B*|), the vector components of the magnetic field in the GSE-coordinate system, the elevation (theta), and azimuthal (phi) of the field direction in the GSE-coordinate system, the suprathermal electron pitch angle distribution, solar wind speed (V_{SW}), proton density (N_p), proton temperature (T_p), ratio of proton thermal pressure to magnetic pressure (β), and the D_{st} index from WDC. The red dashed lines denote the arrival time of the shock. The gray shades show the region of the ICMEs magnetic cloud. Courtesy of figure http://space.ustc.edu.cn/dreams/wind_icmes/index.php.

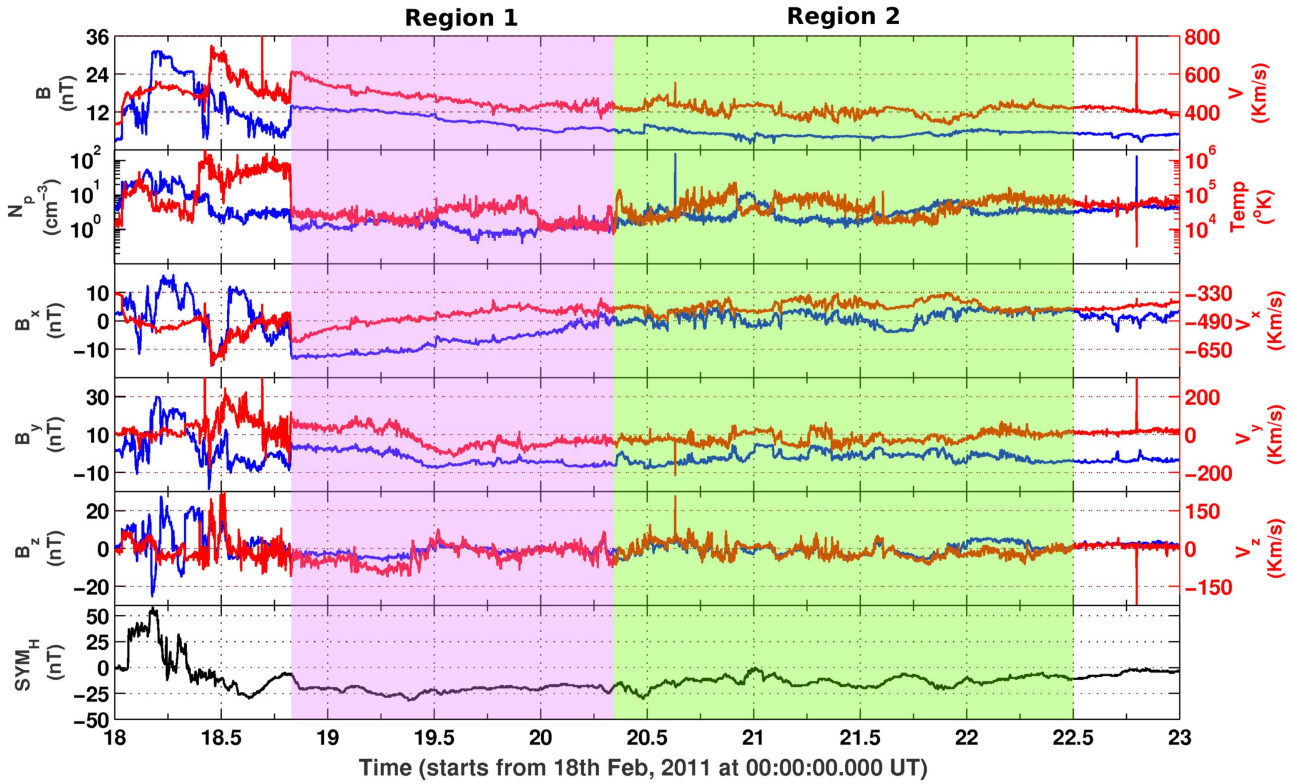

Figure 2. From top to bottom, the first panel shows the magnetic field strength ($|B|$) and solar wind speed (V_{SW}), the second panel shows proton density (N_p) and proton temperature (T_p), and the third, fourth, and fifth panels show the vector components of the magnetic field and solar wind velocity in GSE-coordinate system respectively (data taken from Wind satellite with time cadence of 92 s). The bottom panel shows the SYM_H profile (data taken from Omni database with 60 s time resolution). The pink shaded region is the MC-like structure and green shaded region is the trailing solar wind after the CME.

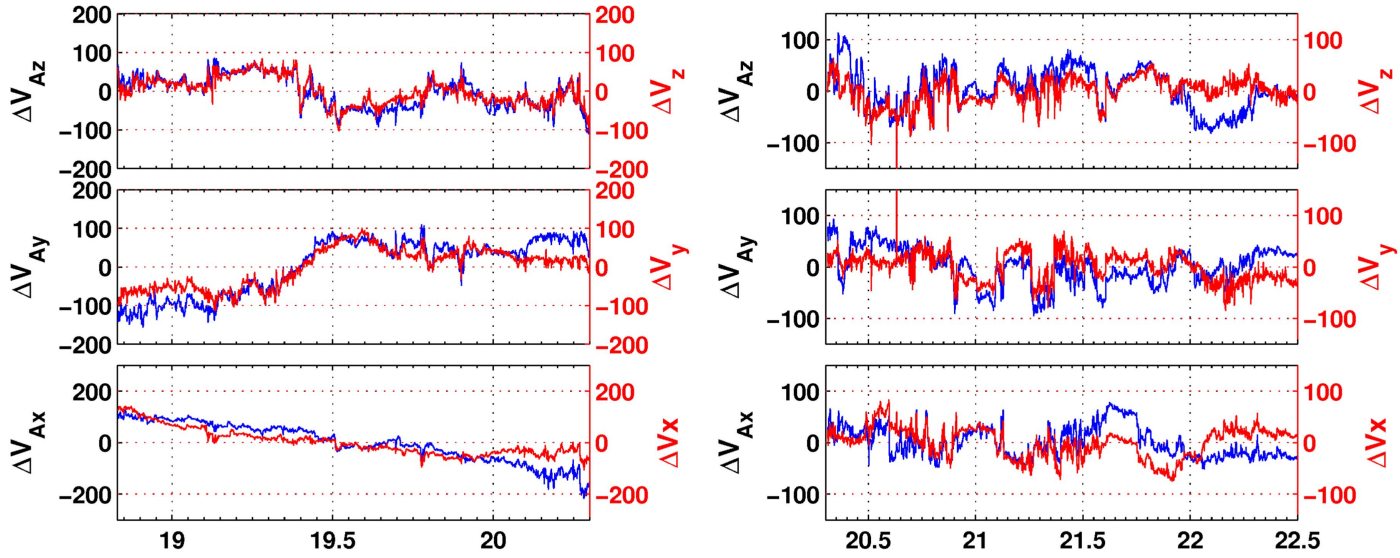

Figure 3. Right three panels (region 1) and left three panels (region 2) illustrate the relative fluctuation of Alfvén velocity vector ΔV_A (blue lines) and that of the proton flow velocity vector ΔV (red lines). (Time cadence of 92 s.)

anisotropy, one can ignored anisotropy in the solar wind; therefore, we usually take $A = \pm 1$ (Yang et al. 2016). The fluctuations ΔB in B can be obtained by subtracting an average value of B from each measured value. Therefore, the fluctuation in Alfvén velocity is

$$\Delta V_A = \frac{\Delta B}{\sqrt{\mu_0 \rho}}. \quad (2)$$

Furthermore, the fluctuations of proton flow velocity ΔV is estimated by subtracting averaged proton flow velocity from measured values. The top, middle, and bottom panels Figure 3 show the comparisons of x, y, and z components of ΔV_A and ΔV, respectively. The fluctuations seen in Figure 3 for both the regions indicate the presence of a signature of Alfvén waves. However, the visual variations in region 1 appeared to be strongly correlated as compared to region 2.

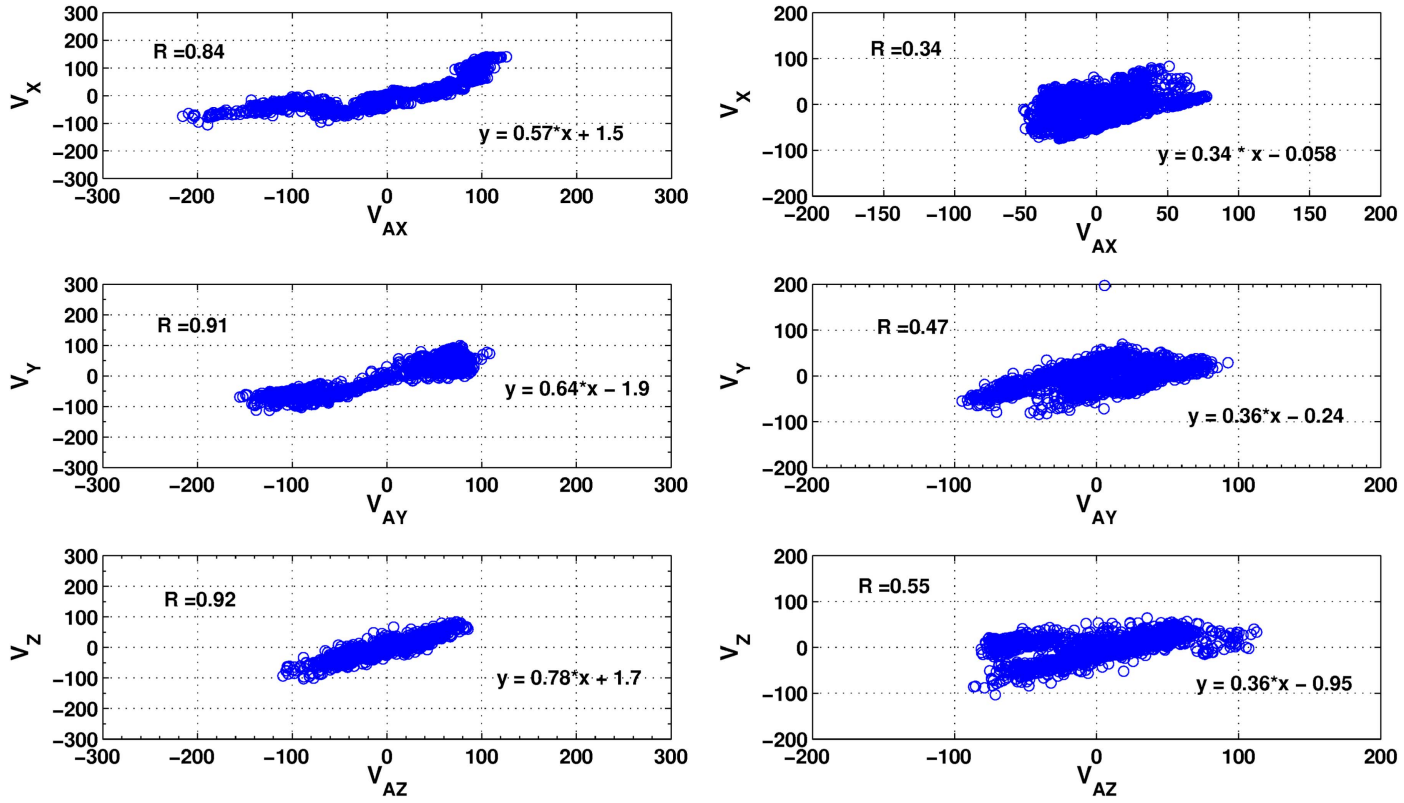

Figure 4. Linear relation between ΔV_A and ΔV for region 1 (left) and region 2 (right) for the event shown in Figure 2. The scattered blue circles are observations from the Wind satellite with a time cadence of 92 s. The R is the correlation coefficient. The equation in each panel suggests the straight-line fit relation between respective components of ΔV_A and ΔV.

Moreover, Figure 4 shows the correlation and linear relation between the fluctuations of Alfvén velocity vector components and the fluctuations of proton flow velocity vector components for both regions 1 and 2 as marked in Figure 2. The linear equations and correlation coefficients are shown in each panel. For region 1, the slopes for *x, y*, and *z* components of three vectors are 0.57, 0.64, and 0.78 and the correlation coefficient (R) between Alfvén and proton flow velocity vector components are noted as 0.84, 0.91, and 0.92, respectively. For region 2, the slopes for three vector components are 0.34, 0.36, and 0.36 and the correlation coefficient between Alfvén and proton flow velocity vector components are 0.34, 0.47, and 0.55, respectively. The correlation coefficients suggest strong positive correlation for region 1, which confirms the Alfvén waves in MC and weak positive correlation for region 2 between ΔV_{Ax} and ΔV_x, ΔV_{Ay} and ΔV_y, ΔV_{Az} and ΔV_z. The MHD static equilibrium suggests that the MC cloud is considered to be strongly coupled plasma under frozen in condition with concentric cylindrical surface layers around the central axis. Therefore, the fluctuations in each layer are mutually connected, which leads to the strong correlation coefficient. However, in trailing solar wind, the heliospheric current sheets are not strongly coupled. Thus, transfer of fluctuations from one sheet to another are not mutually correlated. This leads to a weak correlation coefficient in region 2. In fact, different correlated layers are visible in region 2 of Figure 4. A detailed study of Alfvén fluctuation transfer is needed.

3. Results and Discussion

From our analysis, we find a good correlation between magnetic field and proton velocity vectors. This suggests that magnetic field and fluids are oscillating together in the observed region 1 of the magnetic cloud. Such a scenario means that fluid velocity perturbation is perpendicular to magnetic tension force, which is along the direction of resultant magnetic field. Such a velocity perturbation would lead to magnetic field perturbation and can generate a wave propagating along the direction of tension force. Thus, the wave propagation direction is along the resultant magnetic field direction. This characteristic of the wave is for the torsional Alfvén wave. Thus, our analysis confirms the presence of an Alfvén wave in the magnetic cloud and its weak signature in the trailing solar wind flow.

Earlier studies have shown that HILDCAA events, following a geomagnetic storm, are induced by interplanetary Alfvén waves propagating outward with solar wind. (Tsurutani & Gonzalez 1987; Prestes et al. 2017). The presence of corotating streams containing continuous, large amplitude Alfvén waves causing substorm activity tends to require a long recovery time of several days (Tsurutani et al. 1995a). The associated REDs (relativistic electron events) differentiate between a CME associated storm and a corotating streams associated storm depending on the following parameters: D_{st} index, B_z component, and the solar wind pressure. It was noted that the recovery time for both events was long and the B_z component was fluctuating around zero (Alyana et al. 2007). It is considered that the Alfvén waves may lead to a long duration southward magnetic field and help to provide the energy and

plasma injection to the magnetosphere. However, the Poynting flux observations of the DSMP satellite failed to suggest Alfvén waves as energy input to the magnetic storm and ascribed that the energy input is due to heating of ions and neutral atoms (Huang et al. 2017). Hui & Seyler (1992) have demonstrated that electrons can be accelerated by kinetic Alfvén waves in both hot and cold plasma. The long duration and large amplitude Alfvén waves have the potential to induce different characteristics/profile of geomagnetic storms than that from CMEs and CIRs in the absence of such waves. Thus, Alfvén waves play an important role in the dynamics of space plasma from solar corona to 1 au, and even beyond.

In general, the recovery phase is observed once southward/negative IMF B_z component turns northward/positive (Adebesin 2008). The charge exchange, coulomb scattering and wave–particle interaction are the possible physical mechanisms responsible for the recovery phase (Gonzalez et al. 1994; Daglis et al. 1999). In the charge exchange process, energetic H^+ or O^+ or N^+ ions collide with atmospheric neutral atoms, the ions capture the electrons and become neutralized. The lifetime for the charge exchange process depends upon neutral atomic hydrogen or oxygen density and the equatorial pitch angle of ions. The charge exchange process is important when there are singly charged ions (H^+, O^+, or N^+) with energies up to a few KeV, whereas for higher energies coulomb collision is an important mechanism especially for heavier ions (Daglis et al. 1999). When the recovery time is slow, then wave–particle interaction could be a contributing factor. It is suggested that the pitch angle diffusion by plasma waves also contributes to ring current losses (Daglis et al. 1999). Moreover, it is suspected that during extreme geomagnetic storms, the wave intensities (both proton electromagnetic ion cyclotron waves and electron electromagnetic (chorus) waves) could be substantially greater, resulting in a strong wave–particle interaction. Thus, due to the greater loss cone size and the enhanced wave intensities, rapid ring current losses can occur (Tsurutani et al. 2018). Therefore, wave coherency (Tsurutani et al. 2009; Lakhina et al. 2010; Bellan 2013; Remya et al. 2015) in wave–particle cyclotron resonant interactions should be considered in any updated model explaining the magnetic storm (Tsurutani et al. 2018).

Here, we showed that an unusually long recovery time is observed for a minor geomagnetic storm that was caused by MC of ICME. It is important to note that the B_z component of IMF remained fluctuating near zero throughout regions 1 and 2 (see Figures 1 and 2). We interpret that the long duration of B_z component fluctuations near the zero value is maintained due to the presence of embedded Alfvén waves. Each planetary magnetosphere is considered to be one type of plasmoid in the heliosphere, with a particular orientation of magnetic field. Our earlier study suggested that CME–CME interaction may give rise to magnetohydrodynamic (torsional Alfvén) waves in ICMEs or magnetic clouds, which implied to CME-magnetosphere interaction as well (Raghav & Kule 2018). In a condition of oppositely magnetic orientation of the plasmoids, the magnetic reconnection is the possible physical mechanism for ICME and palsmoid interaction. Thus the present study suggests that the fluctuating B_z fields comprising Alfvén waves are expected to prolong the ring current decay by injecting solar wind energy into the magnetosphere continuously. This is similar to HILDCAAs (Tsurutani & Gonzalez 1987) but caused by magnetic clouds. This indicates that the presence of torsional Alfvén waves may contribute substantially to the geoeffectiveness of solar wind structures, and even the magnetic cloud (Zhang et al. 2014).

The present study demonstrated the presence of Alfvén waves in a magnetic cloud and trailing solar wind flow associated with the CME of February 15th. This CME has interacted with preceding CMEs ejected on February 13th and 14th during its heliospheric evolution. Raghav & Kule (2018) suggested that their interaction may form merged interacting complex ejecta structure and change the force balance conditions of flux ropes, which leads to the generation of the Alfvén wave. It is possible that the interaction of CMEs causes a reconnection between field lines and Alfvén waves may be generated at such a reconnection point. It is also possible that with the steepening of a magnetosonic wave, which forms the shock at the leading edge, could create a trailing Alfvén wave (Tsurutani et al. 1988, 2011). Besides this, it has been suggested that Alfvén waves may be generated in the interplanetary space (Hellinger & Trávníček 2008) and they have been observed in the solar wind propagating outward from the Sun. However, in that case, it would be difficult for the Alfvén wave to get into the MC. Further studies are required to understand the distribution of Alfvén waves and turbulence features in the magnetic clouds.

We conclude that the torsional Alfvén waves play a significant role during the interaction of CME and planetary magnetosphere, they may significantly contribute in geoeffectiveness and recovery time of geomagnetic storms. More studies are required to confirm whether or not a majority of magnetic clouds embedded with Alfvén waves lengthen the recovery phase of geomagnetic storms. Also, this suggest that one needs to consider energy injection by Alfvén waves during the recovery phase in addition to other loss processes like charge exchange, wave–particle interactions, etc. Further studies are required to investigate if the Alfvén waves in ICMEs/MC and within CIRs have different characteristics, possibly because of different plasma beta values in different solar wind structures, and how the geoeffectiveness is different for them.

We are thankful to *WIND* Spacecraft data providers (wind.nasa.gov) for making interplanetary data available. We are also thankful to the Department of Physics (Autonomous), University of Mumbai, for providing us with facilities for the fulfillment of this work. A.R. also thanks the Solar-TErrestrial Physics (STEP) group, USTC, China & SCOSTEP visiting Scholar program. W.M. is supported by the Chinese Academy of Sciences (CAS) Presidents International Fellowship Initiative (PIFI) grant No. 2015PE015 and National Natural Science Foundation of China (NSFC) grant No. 41750110481. A.B. is supported by the NASA Living With a Star Jack Eddy Postdoctoral Fellowship Program, administered by UCARs Cooperative Programs for the Advancement of Earth System Science (CPAESS)."

ORCID iDs

Anil N. Raghav https://orcid.org/0000-0002-4704-6706
Ankush Bhaskar https://orcid.org/0000-0003-4281-1744
Wageesh Mishra https://orcid.org/0000-0003-2740-2280

References

Adebesin, B. 2008, Afr. Rev. Phys., 2, 0017, http://forum.aphysrev.org/index.php/aphysrev/article/viewFile/129/54
Alyana, R., Rajaram, G., Rathod, J., et al. 2007, BASI, 35, 539

Axford, W. 1964, P&SS, 12, 45
Banerjee, D., Pérez-Suárez, D., & Doyle, J. 2009, A&A, 501, L15
Banerjee, D., Teriaca, L., Doyle, J., & Wilhelm, K. 1998, A&A, 339, 208
Behannon, K., Burlaga, L., & Hewish, A. 1991, JGRA, 96, 21213
Behannon, K., & Ness, N. 1966, JGR, 71, 2327
Bellan, P. 2013, PhPl, 20, 042117
Borovsky, J. E., & Denton, M. H. 2006, JGRA, 111, A07S08
Burlaga, L., & Lepping, R. 1977, P&SS, 25, 1151
Cane, H., & Richardson, I. 1997, JGRA, 102, 17445
Cannon, P., Angling, M., Barclay, L., et al. 2013, Extreme Space Weather: Impacts on Engineered Systems and Infrastructure (London: Royal Academy of Engineering)
Carrington, R. C. 1859, MNRAS, 20, 13
Daglis, I. A., Thorne, R. M., Baumjohann, W., & Orsini, S. 1999, RvGeo, 37, 407
Du, A., Tsurutani, B., & Sun, W. 2008, JGRA, 113, A10214
Fan, Y. 2009, ApJ, 697, 1529
Gawali, P., Bhaskar, A., Dhar, A., & Ramesh, D. S. 2016, SpWea, 14, 324
Gonzalez, W., Joselyn, J., Kamide, Y., et al. 1994, JGRA, 99, 5771
Gonzalez, W. D., Tsurutani, B. T., & de Gonzalez, A. L. C. 1999, SSRv, 88, 529
Gosling, J., Teh, W.-L., & Eriksson, S. 2010, ApJL, 719, L36
Hajra, R., Echer, E., Tsurutani, B., & Gonzalez, W. 2013, JGRA, 118, 5626
Hajra, R., Tsurutani, B. T., Echer, E., & Gonzalez, W. D. 2014, GeoRL, 41, 1876
Hajra, R., Tsurutani, B. T., Echer, E., Gonzalez, W. D., & Santolik, O. 2015, ApJ, 799, 39
Harrison, R., Hood, A., & Pike, C. 2002, A&A, 392, 319
Hellinger, P., & Trávníček, P. M. 2008, JGRA, 113, A10109
Huang, C. Y., Huang, Y., Su, Y.-J., Hairston, M. R., & Sotirelis, T. 2017, JASTP, 164, 294
Hudson, P. 1971, P&SS, 19, 1693
Hui, C.-H., & Seyler, C. 1992, JGRA, 97, 3953
Lakhina, G., Tsurutani, B., Gonzalez, W., & Alex, S. 2007, in Encyclopedia of Geomagnetism and Paleomagnetism (Berlin: Springer), 404
Lakhina, G., Tsurutani, B., Verkhoglyadova, O., & Pickett, J. 2010, JGRA, 115, A00F15
Lakhina, G. S., & Tsurutani, B. T. 2016, GSL, 3, 5
Lepping, R., Burlaga, L., Szabo, A., et al. 1997, JGRA, 102, 14049
Maričić, D., Vršnak, B., Dumbović, M., et al. 2014, SoPh, 289, 351
Mishra, W., & Srivastava, N. 2014, ApJ, 794, 64
Osella, A., Favetto, A., & López, E. 1998, JAG, 38, 219
Parker, E. 1958, PhFl, 1, 171
Prestes, A., Klausner, V., & Ojeda-González, A. 2017, AnGeo, 35, 1231
Raghav, A., Bhaskar, A., Lotekar, A., Vichare, G., & Yadav, V. 2014, JCAP, 10, 074
Raghav, A., Shaikh, Z., Bhaskar, A., Datar, G., & Vichare, G. 2017, SoPh, 292, 99
Raghav, A. N., & Kule, A. 2018, MNRAS, 476, L6
Remya, B., Tsurutani, B., Reddy, R., Lakhina, G., & Hajra, R. 2015, JGRA, 120, 7536
Schrijver, C. J., & Siscoe, G. L. 2010, Heliophysics: Space Storms and Radiation: Causes and Effects (Cambridge: Cambridge Univ. Press)
Smith, E. J., & Wolfe, J. H. 1976, GeoRL, 3, 137
Temmer, M., Veronig, A., Peinhart, V., & Vršnak, B. 2014, ApJ, 785, 85
Tian, H., Yao, S., Zong, Q., He, J., & Qi, Y. 2010, ApJ, 720, 454
Tsurutani, B., Gonzalez, W., Lakhina, G., & Alex, S. 2003, JGRA, 108, 1268
Tsurutani, B., Lakhina, G., Verkhoglyadova, O. P., et al. 2011, JASTP, 73, 5
Tsurutani, B. T., & Gonzalez, W. 1995, GeoRL, 22, 663
Tsurutani, B. T., & Gonzalez, W. D. 1987, P&SS, 35, 405
Tsurutani, B. T., & Gonzalez, W. D. 1997, The Interplanetary Causes of Magnetic Storms: A Review (New York: Wiley)
Tsurutani, B. T., Gonzalez, W. D., Gonzalez, A. L., et al. 1995a, JGRA, 100, 21717
Tsurutani, B. T., Gonzalez, W. D., Gonzalez, A. L., et al. 2006, JGRA, 111, A07S01
Tsurutani, B. T., Gonzalez, W. D., Tang, F., Akasofu, S. I., & Smith, E. J. 1988, JGRA, 93, 8519
Tsurutani, B. T., Gonzalez, W. D., Tang, F., & Lee, Y. T. 1992, GeoRL, 19, 73
Tsurutani, B. T., Ho, C. M., Arballo, J. K., Goldstein, B. E., & Balogh, A. 1995b, GeoRL, 22, 3397
Tsurutani, B. T., Lakhina, G. S., Echer, E., et al. 2018, JGRA, 123, 1388
Tsurutani, B. T., Verkhoglyadova, O. P., Lakhina, G. S., & Yagitani, S. 2009, JGRA, 114, A03207
Vichare, G., Alex, S., & Lakhina, G. 2005, JGRA, 110, A03204
Walén, C. 1944, ArA, 30, 1
Yang, L., Lee, L., Chao, J., et al. 2016, ApJ, 817, 178
Zhang, X.-Y., Moldwin, M., Steinberg, J., & Skoug, R. 2014, JGRA, 119, 3259